The Relationship between Age of Air and the Diabatic Circulation of the Stratosphere

MARIANNA LINZ

Massachusetts Institute of Technology–Woods Hole Oceanographic Institution Joint Program in Physical Oceanography, Massachusetts Institute of Technology, Cambridge, Massachusetts

R. ALAN PLUMB

Department of Earth, Atmospheric and Planetary Sciences, Massachusetts Institute of Technology, Cambridge, Massachusetts

EDWIN P. GERBER

Courant Institute of Mathematical Sciences, New York University, New York, New York

ADITI SHESHADRI

Department of Applied Physics and Applied Mathematics, Columbia University, New York, New York

(Manuscript received 21 April 2016, in final form 28 July 2016)

ABSTRACT

The strength of the Brewer–Dobson circulation is difficult to estimate using observations. Trends in the age of stratospheric air, deduced from observations of transient tracers, have been used to identify trends in the circulation, but there are ambiguities in the relationship between age and the strength of the circulation. This paper presents a steady-state theory and a time-dependent extension to relate age of air directly to the diabatic circulation of the stratosphere. In steady state, it is the difference between the age of upwelling and downwelling air through an isentrope and not the absolute value of age that is a measure of the strength of the diabatic circulation through that isentrope. For the time-varying case, expressions for other terms that contribute to the age budget are derived. An idealized atmospheric general circulation model with and without a seasonal cycle is used to test the time-dependent theory and to find that these additional terms are small upon annual averaging. The steady-state theory holds as well for annual averages of a seasonally varying model as for a perpetual-solstice model. These results are a step toward using data to quantify the strength of the diabatic circulation.

1. Introduction

The Brewer–Dobson circulation (BDC) is the slow meridional overturning circulation of the stratosphere, consisting of upwelling through the tropical tropopause, then poleward motion and downwelling through the midlatitudes and at the poles. This circulation is critical for the vertical transport of tracers such as ozone, volcanic aerosols, and chlorofluorocarbons (CFCs); for the temperature of the tropical tropopause and consequently the amount of water vapor in the stratosphere; and for stratosphere–troposphere exchange [e.g., Butchart (2014) and references therein]. Stratosphere-resolving climate models show a positive trend in the BDC—an increase in the tropical upwelling at a fixed pressure level—as a robust response to increasing greenhouse gases (Butchart et al. 2006; Hardiman et al. 2014). This increasing trend in the residual circulation, however, might better be described as a ''lifting'' trend, associated with the upward expansion of the tropopause (and entire tropospheric circulation) in response to global warming (Singh and O'Gorman 2012; Oberländer-Hayn et al. 2016). Reanalysis products are in qualitative agreement with the

Corresponding author address: Marianna Linz, Massachusetts Institute of Technology, 77 Massachusetts Ave., 54-1615, Cambridge, MA 02139.
E-mail: mlinz@mit.edu

DOI: 10.1175/JAS-D-16-0125.1

© 2016 American Meteorological Society

climate models, showing positive trends over the period 1979–2012, but with differing spatial structures for each individual product (Abalos et al. 2015). Satellite-derived temperature trends are also consistent with the model predictions (Fu et al. 2015).

The mean age of air (Hall and Plumb 1994; Waugh and Hall 2002) has been used as a metric for models' abilities to reproduce the stratospheric circulation (e.g., Hall et al. 1999; Butchart et al. 2011). The apparent increase in the residual circulation has led to predictions that the mean age of air should decrease. Attempts to identify trends of decreasing age of air from observations of transient tracers in the stratosphere have found little evidence; in fact, age appears to be mostly increasing (Engel et al. 2009; Stiller et al. 2012; Haenel et al. 2015). However, for one thing, available data records are short enough—global satellite coverage of age tracers is available for less than a decade—that apparent trends could be indicative of interannual variability rather than of long-term trends (cf. Garcia et al. 2011). Moreover, mean age is a statistical average over many transport pathways (Hall and Plumb 1994), and at a given location it depends on mixing processes and not just mean advection (Waugh and Hall 2002; Garny et al. 2014; Ploeger et al. 2015a). Satellite observations of SF_6 have been used to identify spatially inhomogeneous trends in age between 2002 and 2012 (Stiller et al. 2012; Haenel et al. 2015), and while these trends can be compared to model output, for which the contributions of advection and mixing can be isolated (Ploeger et al. 2015b), in reality they are difficult to disentangle (Ray et al. 2010).

There are certain aspects of the stratospheric age distribution that are dependent on the mean circulation alone. Using a "leaky tropical pipe" model, Neu and Plumb (1999) showed that, in steady state, the tropics minus midlatitude age difference on an isentrope depends only on the overturning mass flux and is independent of isentropic mixing, provided that diabatic mixing is negligible. This result has been used to assess transport in chemistry–climate models (Strahan et al. 2011). Here we present a generalization of this analysis. In section 2a, we show that the steady-state result of a simple and direct relationship between age gradient and overturning diabatic mass flux holds even in the absence of a "tropical pipe," provided the isentropic age gradient is defined appropriately. For the more realistic case of an unsteady circulation, we show in section 2b that the result holds for the time average; in section 2c, the fully transient case is discussed. The accuracy of the theoretical predictions is demonstrated in section 3 using results from a simple general circulation model; the theory works well when applied to multiyear averages, though there are systematic discrepancies that appear to indicate a role for large-scale diabatic diffusion. Applications and limitations of the theory are discussed in section 4.

2. Age difference theory

A passive tracer χ follows the tracer continuity equation:

$$\frac{\partial \chi}{\partial t} + \mathcal{L}(\chi) = \mathcal{S}, \tag{1}$$

where $\mathcal{L}$ is the advection–diffusion operator and $\mathcal{S}$ is the source. For the stratospheric age tracer Γ, the source is 1 (yr yr^{-1}) with a boundary condition of $\Gamma = 0$ at the tropopause. In equilibrium, age determined from a conservative tracer ($\mathcal{S} = 0$) with a boundary condition that is linearly growing at the tropopause will be equivalent to the age tracer Γ (Waugh and Hall 2002). Considering the tracer continuity equation for the age tracer Γ in potential temperature (θ) coordinates, we rewrite the full advection–diffusion operator as the divergence of a flux to obtain

$$\frac{\partial}{\partial t}(\sigma\Gamma) + \nabla \cdot \mathbf{F}^{\Gamma} = \sigma, \tag{2}$$

where $\sigma = -(1/g)(\partial p/\partial\theta)$ is the isentropic density and $\mathbf{F}^{\Gamma}$ is the advective–diffusive flux of age.

a. Steady state

In a steady state, integrating (2) over the volume $\mathcal{V}$ above any surface $\mathcal{S}$ shows that

$$\int_{\mathcal{S}} \mathbf{n} \cdot \mathbf{F}^{\Gamma}\, dA = \int_{\mathcal{V}} \sigma\, dA\, d\theta = \int_{\mathcal{V}} \rho\, dV, \tag{3}$$

where $\mathbf{n}$ is the downward unit normal to the surface $\mathcal{S}$ and assuming hydrostatic balance. The net age flux through a surface is equal to the mass above that surface so that, for example, the age flux through the tropopause is equal to the mass of the stratosphere and the rest of the atmosphere above (Volk et al. 1997; Plumb 2002).

Let us choose $\mathcal{S}$ to be an isentropic surface that is entirely within the stratosphere. If the motions are strictly adiabatic, isentropic stirring will cause no flux through the surface. Assuming diabatic diffusion of age is negligible, the diabatic transport is entirely advective, and (3) gives

$$\int_{\theta} \sigma\dot{\theta}\Gamma\, dA = -M(\theta), \tag{4}$$

where $\int_{\theta}$ is the integral over the θ surface and $M(\theta) = \int_{\mathcal{V}} \rho\, dV$ is the mass above the θ surface. We

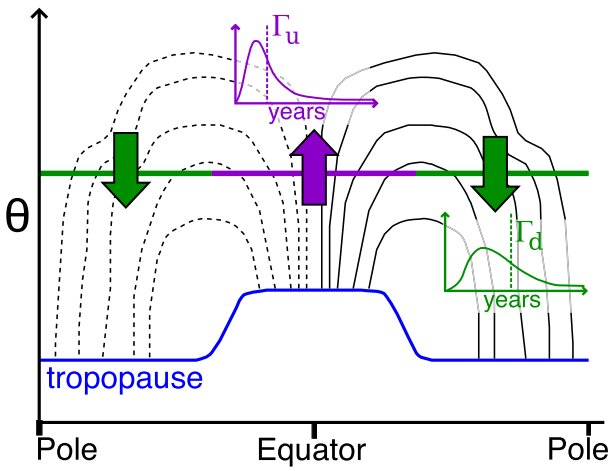

FIG. 1. A schematic diagram of the time-average circulation of the stratosphere and the overturning through one isentrope. The diabatic circulation streamfunction is sketched in the black contours. The upwelling region of the isentrope is purple, and the downwelling region is green. (insets) The age spectra are shown schematically for the upwelling and downwelling air, along with the means, Γ_u and Γ_d. Based on a similar diagram in Waugh and Hall (2002).

define the mass-flux-weighted age of upwelling and downwelling air as

$$\Gamma_u(\theta) = \left(\int_{\mathrm{up}} \sigma\dot{\theta}\, dA\right)^{-1} \int_{\mathrm{up}} \sigma\dot{\theta}\Gamma\, dA, \tag{5}$$

and

$$\Gamma_d(\theta) = \left(\int_{\mathrm{down}} \sigma\dot{\theta}\, dA\right)^{-1} \int_{\mathrm{down}} \sigma\dot{\theta}\Gamma\, dA, \tag{6}$$

where $\int_{\mathrm{up}}$ and $\int_{\mathrm{down}}$ are integrals over the portion of the area of the isentropic surface through which air is upwelling and downwelling, respectively, as shown in Fig. 1. Although this schematic is for a zonal mean, the regions are defined in two dimensions and not simply by the zonal-mean turnaround latitudes. While the schematic shows upwelling in the tropics and downwelling in the extratropics, nothing in the derivation presented here requires any particular structure for the diabatic circulation, provided only that it is nonzero.

In equilibrium under steady-state conditions, the mass flux through the upwelling and downwelling areas must be equal, and let this be called $\mathcal{M}(\theta)$:

$$\int_{\mathrm{up}} \sigma\dot{\theta}\, dA = -\int_{\mathrm{down}} \sigma\dot{\theta}\, dA = \mathcal{M}(\theta). \tag{7}$$

Then

$$\int_{\mathrm{up}} \sigma\dot{\theta}\Gamma\, dA = \mathcal{M}\Gamma_u; \tag{8}$$

$$\int_{\mathrm{down}} \sigma\dot{\theta}\Gamma\, dA = -\mathcal{M}\Gamma_d. \tag{9}$$

The global integral in (4) is the sum of (8) and (9):

$$\int_{\theta} \sigma\dot{\theta}\Gamma\, dA = \mathcal{M}(\Gamma_u - \Gamma_d) = -M(\theta), \tag{10}$$

which can be rewritten as

$$\Delta\Gamma(\theta) = \Gamma_d(\theta) - \Gamma_u(\theta) = \frac{M(\theta)}{\mathcal{M}(\theta)}. \tag{11}$$

Thus, the gross mass-flux-weighted age difference, as defined by (11), (5), and (6), between downwelling and upwelling air is simply the ratio of the mass above the isentrope to the mass flux through it: that is, the gross residence time of the air above the surface.

This relationship is essentially identical to that obtained by Neu and Plumb (1999) in their tropical pipe model, but the present approach avoids assumptions made in that model, other than steadiness and the neglect of diabatic diffusion (both of which will be addressed in the following sections). As discussed by those authors [and by Plumb (2002) and Waugh and Hall (2002)], (11) is remarkable and counterintuitive in that the gross isentropic age gradient is independent of isentropic mixing (except insofar as the mixing of potential vorticity drives the diabatic circulation) and depends only on the overturning mass flux through the θ surface; it is independent of path in the diabatic circulation. For a given mass flux, the age gradient is the same whether the circulation is deep or shallow.

The potential power of (11) lies in the fact that, unlike age itself, $\Delta\Gamma$ is a measure of the age distribution that is directly dependent only on the overturning mass flux and hence provides a tracer-based means of quantifying the strength of the circulation. The one isentrope on which the age itself is relevant is that which skims the tropical tropopause; there $\Gamma_u \approx 0$, and so $\Gamma_d \approx \Delta\Gamma$. Below this isentrope (i.e., in the lowermost stratosphere), (11) is no longer applicable as the assumptions made (in particular, the neglect of diabatic diffusion) do not apply where portions of the isentropes are below the tropopause.

b. Time average

The atmosphere is not in steady state; the stratospheric circulation varies on synoptic, seasonal, and interannual time scales. We can instead consider the time-average age equation. The time derivative in (2) goes to zero for a

long-enough averaging period, provided the trends are small. Then (4) becomes

$$\overline{\int_\theta \sigma\dot{\theta}\Gamma\, dA}^t = -\overline{M(\theta)}^t, \tag{12}$$

where $\overline{\cdots}^t$ is the time mean. We can define the time-average mass-flux-weighted age of upwelling and of downwelling air as follows:

$$\Gamma_{\overline{u}}(\theta) = \left[\overline{\int_{\overline{\mathrm{up}}^t} \sigma\dot{\theta}\, dA}^t\right]^{-1} \overline{\int_{\overline{\mathrm{up}}^t} \sigma\dot{\theta}\Gamma\, dA}^t, \tag{13}$$

and

$$\Gamma_{\overline{d}}(\theta) = \left[\overline{\int_{\overline{\mathrm{down}}^t} \sigma\dot{\theta}\, dA}^t\right]^{-1} \overline{\int_{\overline{\mathrm{down}}^t} \sigma\dot{\theta}\Gamma\, dA}^t, \tag{14}$$

where now the upwelling region is defined by where the time-average diabatic vertical velocity is positive ($\overline{\dot{\theta}}^t > 0$). When we equivalently define the mass flux as

$$\overline{\int_{\overline{\mathrm{up}}^t} \sigma\dot{\theta}\, dA}^t = -\overline{\int_{\overline{\mathrm{down}}^t} \sigma\dot{\theta}\, dA}^t = \overline{\mathcal{M}(\theta)}^t, \tag{15}$$

this allows us to write (12) as

$$\overline{\int_\theta \sigma\dot{\theta}\Gamma\, dA}^t = \overline{\mathcal{M}}^t(\Gamma_{\overline{u}} - \Gamma_{\overline{d}}) = -\overline{M(\theta)}^t, \tag{16}$$

or

$$(\Gamma_{\overline{d}} - \Gamma_{\overline{u}}) = \frac{\overline{M(\theta)}^t}{\overline{\mathcal{M}}^t}. \tag{17}$$

With time averaging, we thus recover the form of the result from the steady-state theory.

Although this derivation has been done for upwelling and downwelling regions, the time-average formulation does not require the two regions of the isentrope to be strictly upwelling or downwelling. As long as the isentrope is split into only two regions that together span the surface, any division will do. The overturning mass flux $\overline{\mathcal{M}(\theta)}^t$ will be the net mass flux up through one region and down through the other. For example, the "upwelling" could be defined as 20°S–20°N and the "downwelling" as the rest of the isentrope. The difference between the mass-flux-weighted age averaged over the area outside of 20°S–20°N and averaged over the area within 20°S–20°N would give the total overturning mass flux through those regions. Because some of the true upwelling is now in the "downwelling" region, the total overturning mass flux between these two regions will be necessarily less than the true total overturning mass flux through the surface. We will demonstrate this and discuss further in section 3. We emphasize that the "age difference" in all of these cases is based on the mass-flux-weighted average ages; hence, in principle, it is necessary to know the circulation in order to accurately calculate the age difference as defined here.

c. *Time varying*

Here we use a different approach that allows us to look at seasonal variability and fully account for time variations. The upwelling and downwelling mass fluxes are not necessarily equal, and the mass above the isentrope may be changing. The age at a given location can also change in time. Returning to the ideal age equation, (2), integrating over the volume above an isentropic surface, there is now an additional time-dependent term:

$$\int_\theta \sigma\dot{\theta}\Gamma\, dA = -M(\theta) + \frac{\partial}{\partial t}\left[\int \Gamma\, dM\right], \tag{18}$$

where

$$\int \Gamma\, dM = \int_{\mathcal{V}} \sigma\Gamma\, dA\, d\theta \tag{19}$$

is the mass-integrated age above the isentrope. This term accounts for fluctuations in the mass-weighted total age above the isentrope. If the mass above the isentrope is varying in time,

$$\mathcal{M}_d + \mathcal{M}_u = \frac{\partial M}{\partial t}. \tag{20}$$

The upwelling and downwelling regions can also be varying in time and must now be defined instantaneously. Define the total overturning circulation

$$\mathcal{M}(\theta) = (\mathcal{M}_u - \mathcal{M}_d)/2, \tag{21}$$

recalling that $\mathcal{M}_u > 0$ and $\mathcal{M}_d < 0$ so that $\mathcal{M}(\theta)$ is always positive. From (20) and (21), we write

$$\mathcal{M}_u = \mathcal{M}(\theta) + \frac{1}{2}\frac{\partial M}{\partial t} \tag{22}$$

and

$$\mathcal{M}_d = -\mathcal{M}(\theta) + \frac{1}{2}\frac{\partial M}{\partial t}. \tag{23}$$

Then we rewrite the flux equations, (8) and (9):

$$\int_{\mathrm{up}} \sigma\dot{\theta}\Gamma\, dA = \mathcal{M}_u\Gamma_u = \Gamma_u\left[\mathcal{M}(\theta) + \frac{1}{2}\frac{\partial M}{\partial t}\right], \tag{24}$$

and

$$\int_{\text{down}} \sigma\dot{\theta}\Gamma\, dA = \mathcal{M}_d\Gamma_d = -\Gamma_d\left[\mathcal{M}(\theta) - \frac{1}{2}\frac{\partial M}{\partial t}\right]. \tag{25}$$

As in the steady-state case, the net global flux is the sum of these two. Using (18), the time-dependent version of (10) is

$$\mathcal{M}\Delta\Gamma - M = -(M\Gamma_s)_t + \frac{1}{2}(\Gamma_u + \Gamma_d)\frac{\partial M}{\partial t}, \tag{26}$$

where $\Delta\Gamma = \Gamma_d - \Gamma_u$ as before, and

$$\Gamma_s(\theta) = \frac{1}{M}\int_\theta \Gamma\, dM \tag{27}$$

is the mean age of air above the isentrope. The two terms on the right side of (26) arise because the time derivatives are no longer zero. Throughout the rest of the paper, these two terms will be collectively referred to as the "time-derivative terms."

The balance expressed by (26) should hold true at any time. However, averaging over a year or several years will make the time derivatives smaller, as the high-frequency variability and seasonal cycle are stronger than the interannual variability. The time derivatives will now be expressed with a subscript. Rearranging and taking the time average gives

$$\overline{\mathcal{M}\Delta\Gamma}^t = \overline{M}^t - \overline{(M\Gamma_s)_t}^t + \frac{1}{2}\overline{M_t(\Gamma_u + \Gamma_d)}^t. \tag{28}$$

Separating the overturning $\mathcal{M}$ and the age difference $\Delta\Gamma$ into time-mean components and deviations therefrom ($\mathcal{M} = \overline{\mathcal{M}}^t + \mathcal{M}'$ and $\Delta\Gamma = \overline{\Delta\Gamma}^t + \Delta\Gamma'$) yields

$$\overline{\mathcal{M}}^t\overline{\Delta\Gamma}^t = \overline{M}^t - \overline{\mathcal{M}'\Delta\Gamma'}^t - \overline{(M\Gamma_s)_t}^t + \frac{1}{2}\overline{M_t(\Gamma_u + \Gamma_d)}^t, \tag{29}$$

or

$$\overline{\Delta\Gamma}^t = \frac{\overline{M}^t}{\overline{\mathcal{M}}^t} - \frac{\overline{\mathcal{M}'\Delta\Gamma'}^t}{\overline{\mathcal{M}}^t} - \frac{\overline{(M\Gamma_s)_t}^t}{\overline{\mathcal{M}}^t} + \frac{1}{2}\frac{\overline{M_t(\Gamma_u + \Gamma_d)}^t}{\overline{\mathcal{M}}^t}. \tag{30}$$

If the time-derivative terms and the term involving fluctuations $\overline{\mathcal{M}'\Delta\Gamma'}^t$ are small, then we arrive at the same result as in steady state, and the age difference is the mean residence time in the region above the isentrope.

Note that this differs from the time-average version of the theory, presented in section 2b. In the derivation of (30), the average of $\Delta\Gamma$ is taken after calculating the mass-flux-weighted upwelling and downwelling ages instantaneously. The time-varying theory is sensitive to the definition of region of upwelling/downwelling, in contrast to the time-average theory, because the instantaneous mass flux averaged over either the upwelling or downwelling region could change sign in time. If the flux were zero in one region and nonzero in the other, then because of the mass-flux weighting, $\Delta\Gamma$ would be singular. In contrast, the time-average mass flux through a region as defined in (17) will be well defined as long as the regions are defined to have nonzero overturning mass flux. The time-varying theory is therefore only appropriate when the upwelling and downwelling regions are defined instantaneously.

3. Verification in a simple atmospheric GCM

a. Model setup

To verify the theory, we evaluate the terms in (11), (17), and (26) in a simple atmospheric GCM with and without a seasonal cycle. The model is a version of the dynamical core developed at the Geophysical Fluid Dynamics Laboratory (GFDL). It is dry and hydrostatic, with radiation and convection replaced with Newtonian relaxation to a zonally symmetric equilibrium temperature profile. We use 40 hybrid vertical levels that are terrain following near the surface and transition to pressure levels by 115 hPa. Unlike previous studies using similar idealized models (e.g., Polvani and Kushner 2002; Kushner and Polvani 2006; Gerber and Polvani 2009; Gerber 2012; Sheshadri et al. 2015), the model solver is not pseudospectral. It is the finite-volume dynamical core used in the GFDL Atmospheric Model, version 3, (AM3; Donner et al. 2011), the atmospheric component of GFDL's CMIP5 coupled climate model. The model utilizes a cubed-sphere grid (Putman and Lin 2007) with "C48" resolution, where there is a 48 × 48 grid on each side of the cube, and so roughly equivalent to a 2° × 2° resolution. Before analysis, all fields are interpolated to a regular latitude–longitude grid using code provided by GFDL.

In the troposphere, the equilibrium temperature profile is constant in time and similar to Held and Suarez (1994) with the addition of a hemispheric asymmetry in the equilibrium temperature gradient that creates a colder Northern Hemisphere [identical to Polvani and Kushner (2002)]. In the polar region (50°–90°N/S), the equilibrium temperature profile decreases linearly with height with a fixed lapse rate γ, which sets the strength of the stratospheric polar vortex. The stratospheric thermal relaxation time scale is 40 days. As an analog for the planetary-scale waves generated by land–sea contrast, flow over topography, and nonlinear interactions

TABLE 1. Summary of setup for the five runs used in this study. One run has a seasonal cycle as described in the text, and the others are perpetual solstice with varying stratospheric lapse rates γ (K km^{-1}) and wavenumber-2 topographic forcing h (km) in the one hemisphere only. The winter hemisphere in these perpetual-solstice runs is the same as the hemisphere with topography.

Run No.	Configuration	γ (K km^{-1})	h (km)
1	Seasonally varying	4	4
2	Perpetual solstice	1.5	3
3	Perpetual solstice	4	4
4	Perpetual solstice	4	0
5	Perpetual solstice	5	3

of synoptic-scale eddies, wave-2 topography is included in the Northern Hemisphere at the surface centered at 45°N as in Gerber and Polvani (2009). The Southern Hemisphere has no topography. As in Gerber (2012), a "clock" tracer is specified to increase linearly with time at all levels within the effective boundary layer of the Held and Suarez (1994) forcing (model levels where $p/p_s \geq 0.7$) and is conserved otherwise, providing an age of air tracer.

The seasonally varying run has a seasonal cycle in the stratospheric equilibrium temperature profile following Kushner and Polvani (2006), with a 360-day year consisting of a constant summer polar temperature and sinusoidal variation of the winter polar temperature, so that equilibrium temperature in the polar vortex is minimized at winter solstice. The lapse rate is $\gamma = 4\,\mathrm{K\,km^{-1}}$, and the topography is 4 km high. With a lower stratosphere–troposphere transition, this topographic forcing and lapse rate were found by Sheshadri et al. (2015) to create the most realistic Northern and Southern Hemisphere–like seasonal behavior. The model is run until the age has equilibrated (27 yr) and then for another 50 yr, which provide the statistics for these results.

For the perpetual-solstice runs, the model is run in a variety of configurations, as described in Table 1. These four simulations correspond to those highlighted in detail in Figs. 1–3 of Gerber (2012), capturing two cases with an "older" stratosphere and two cases with a "younger" stratosphere. Note, however, that Gerber (2012) used a pseudospectral model and the age is sensitive to model numerics. All are run to equilibrium, at least 10 000 days, and the final 2000 days are averaged for the results presented here.

b. Model seasonality

Figure 2a shows a 20-yr climatology of the residual vertical velocity at 53 hPa for the seasonally varying model run. Because of artifacts from the interpolation from the cubed-sphere grid and the high frequency of temporal variability, the field has been smoothed in time and latitude using a binomial filter of 2 weeks and 10°.

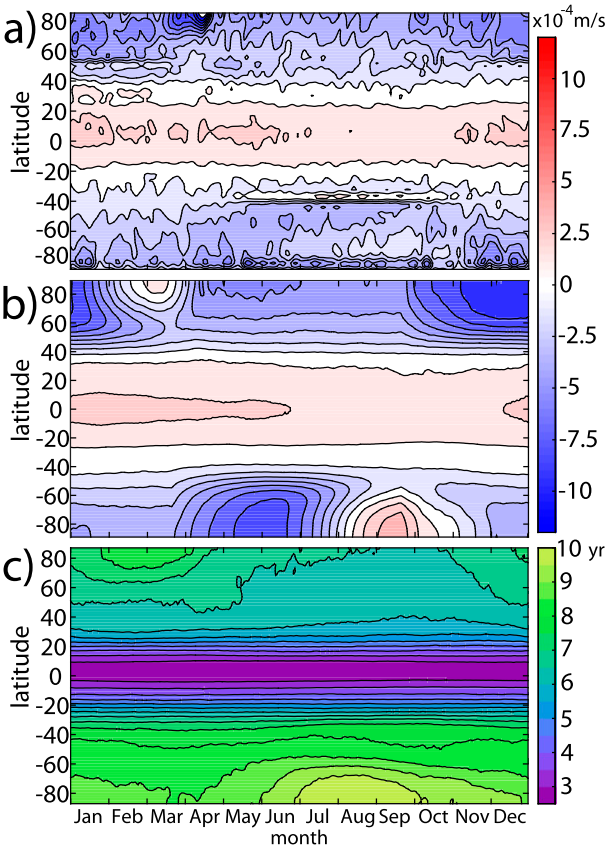

FIG. 2. Annual cycles based on a 20-yr average of the seasonally varying model run. (a) The residual-circulation vertical velocity at 53 hPa. The field has been filtered using a binomial filter (14 days in time and 10° in latitude) in order to smooth high temporal variability and cubed-sphere interpolation artifacts. (b) The zonal-mean diabatic vertical velocity at 500 K divided by the background stratification ($\dot{\theta}/\overline{\theta_z}$). The 500-K isentrope is on the annual average located near the 53-hPa surface. (c) The age on the 500-K isentrope. Contour levels are $1.2 \times 10^{-4}\,\mathrm{m\,s^{-1}}$ and 0.5 yr.

Discontinuities are nevertheless visible in midlatitudes in both hemispheres. The seasonal cycle is barely evident; there is stronger polar downwelling in Northern Hemisphere winter/spring and weaker tropical upwelling during Southern Hemisphere winter. Figure 2b shows the climatology of the zonal-mean diabatic velocity $\dot{\theta}/\overline{\theta}_z$ on the 500-K surface for the same model run. The 500-K surface is, in the annual mean, near the 53-hPa surface. The diabatic vertical velocity is similar to the residual vertical velocity in the annual mean but differs at the equinoxes and has a much stronger seasonal cycle in high latitudes. These differences are primarily a result of the motion of the isentropes over the course of the year; in spring, the isentropes descend as the polar region warms, and hence the air moves upward relative to the isentropes. This strong seasonal variability in the diabatic vertical velocity, the relevant vertical velocity for the

age difference theory, suggests the importance of the time-derivative terms in (26) and (30). Figure 2c shows the climatology of age on the 500-K isentrope for the same run. The ages for this model tend to be older than observed ages, which can be attributed partially to the age being zero at 700 hPa rather than at the tropopause and partially to the strength of the circulation in the model. Nevertheless, the pattern of age is as expected given the circulation; the air is younger in the tropics and older at the poles, with little variability in the tropics and the oldest air in the vortices in late winter. As in observations (Stiller et al. 2012), the Northern Hemisphere air is generally younger than the Southern Hemisphere air. The seasonal variability in age difference, dominated by variability in polar age of air, is also large compared to the variability in the residual vertical velocity. Meanwhile, the total mass above the isentropic surfaces changes very little over the course of the year.

c. *Time-average results*

We examine the time-average theory as described in section 2b. We calculate the terms in (17) for annual averages of 50 yr of the seasonally varying model run and for the average over the last 2000 days of the perpetual-solstice run with the same lapse rate and topography (runs 1 and 3 in Table 1). To demonstrate the flexibility of the definition of "upwelling" and "downwelling" regions, we have calculated $(\Gamma_{\overline{d}} - \Gamma_{\overline{u}})$ and $\overline{M(\theta)}^t / \overline{\mathcal{M}}^t$ for several regions, and these are shown in Fig. 3. The different "upwelling" regions are defined as follows: the "true" upwelling based on the time-averaged location of positive diabatic vertical velocity (this is not uniform in longitude); between 20°S and 20°N; between 30°S and 30°N; and between 40°S and 40°N. For each case, the "downwelling" region is the rest of the globe. The average age in each region ($\Gamma_{\overline{u}}$ or $\Gamma_{\overline{d}}$) is the mass-flux-weighted age through each of these regions as defined in (13) and (14). Three different levels are shown, and error bars are one standard deviation of the annual averages for the seasonally varying model run. The maximum overturning mass flux is for the "true" regions, as expected. Because it is most different from the true region, the 20° overturning is the weakest, indicated by the largest age differences. All of the different regions have similar agreement with the theory in both the seasonally varying model (red and gray points) and in the perpetual-solstice model (blue and teal points). Although the flexibility of the theory is clear from this plot, the 20° tropics do not capture all the upwelling in the model, as can be seen in Fig. 2b. Most of the upwelling occurs in the narrow band between 20°S and 20°N, but the 20° overturning is substantially different from the "true" overturning because the weaker upwelling between 20° and 40° is of older air, and so the age difference neglecting that upwelling is greater than for the "true" regions. Thus, although this method can determine the overturning through two regions, to determine the overturning mass flux through the stratosphere, the "true" regions must be used. The agreement of the 40° tropics with the "true" regions is a reflection that, on average, the "true" regions are bounded by 40° in this simple model. The age difference is largest at 600 K for all of these model runs, which demonstrates a minimum in the relative strength of the overturning circulation. Because the perpetual-solstice version of the model has no weakening and reversing of the circulation associated with the seasonal cycle, the annual-mean overturning mass flux through an isentrope is greater than in the seasonally varying model, and so the age difference is smaller.

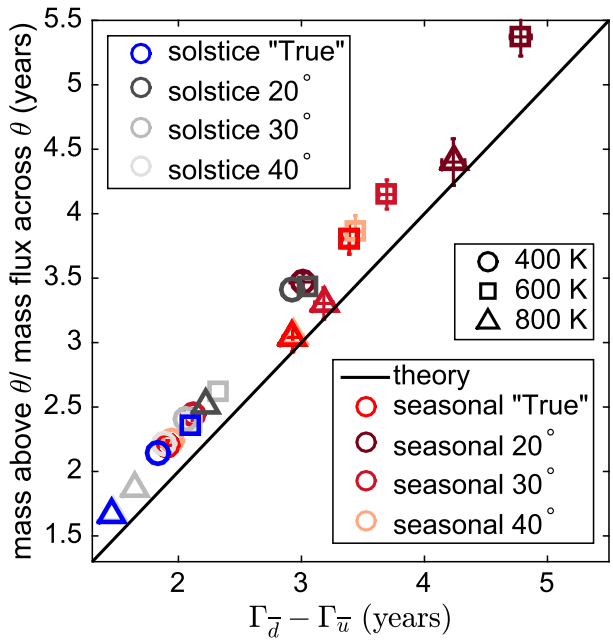

FIG. 3. The ratio of mass above an isentrope to mass flux through an isentrope vs the difference between age of air in different regions on the isentrope. The red and red-toned points are based on the seasonally varying model. The blue and gray points are based on the perpetual-solstice model run with $\gamma = 4\,\mathrm{K\,km^{-1}}$ and 4-km topography. The "true" points in red and blue are calculated using the time-average "true" upwelling and downwelling regions. The gray and red-toned points are calculated with the "upwelling" region as the band between 20°S and 20°N, 30°S and 30°N, and 40°S and 40°N and the "downwelling" region is defined as the rest of the globe. The darker points correspond to narrower tropics for both the seasonally varying and perpetual-solstice runs. Error bars are one standard deviation of the annual averages. The black line is the one-to-one relationship predicted by the theory, and the different symbols are different isentropic levels.

All of the points fall above the one-to-one line, a discrepancy consistent with the neglect of diabatic diffusion in the theory, as will be discussed in section 3f. The points

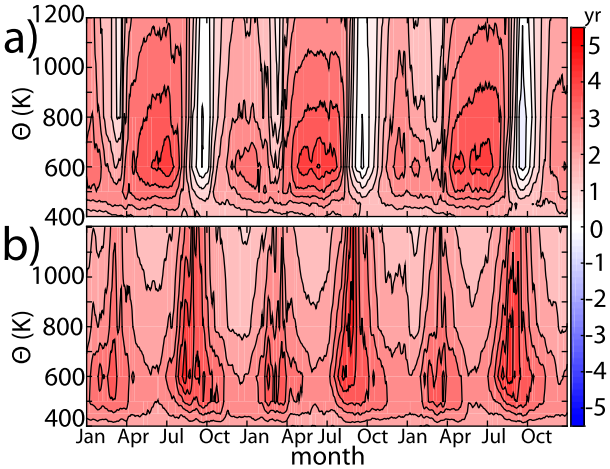

FIG. 4. Three years of (a) the age difference $\Delta\Gamma$ and (b) the ratio of total mass above the isentrope to overturning mass flux through the isentrope $[M(\theta)/\mathcal{M}]$ calculated daily for the seasonally varying model run. Contour levels are 0.5 yr.

on the 800-K isentrope are closest to the theory line, which is also consistent with diabatic diffusion. The results from the seasonally varying model agree as well with the theory as do the results from the perpetual-solstice run, demonstrating the success of the time-average theory in recovering the steady result.

d. Time-varying results

Next we move on to the time-varying theory; consider Fig. 4. Figure 4a shows 3 yr of the age difference, and Fig. 4b shows the total mass divided by the mass flux for the same 3 yr of the seasonally varying model run. If the steady-state theory held instantaneously, these would be equal at all times. They are obviously not equal; in fact, their seasonal cycles are out of phase, with even negative values of age difference when there is polar diabatic upwelling of very old air associated with the final warming event each Southern Hemisphere spring.

We evaluate the time-derivative terms in (26), $(M\Gamma_s)_t$ and $(\Gamma_u + \Gamma_d)M_t/2$. To calculate $(M\Gamma_s)_t$, the mass-weighted average age above each pressure surface is calculated and then interpolated to the isentropes—the integration is performed in pressure coordinates for improved accuracy. The product of the age and the total mass has substantial high-frequency variability. If the model were not run to steady state, long-term changes in the average age of air in the stratosphere would also appear in this term. For example, a relatively dramatic mean age change of 0.5 yr decade^{-1} would make this term about 5% of the size of the total mass above the isentrope. The other term, $(\Gamma_u + \Gamma_d)M_t/2$, has much less short-term variability.

The average seasonal cycle over 20 yr of the model run for each of the terms in (26) is shown for three

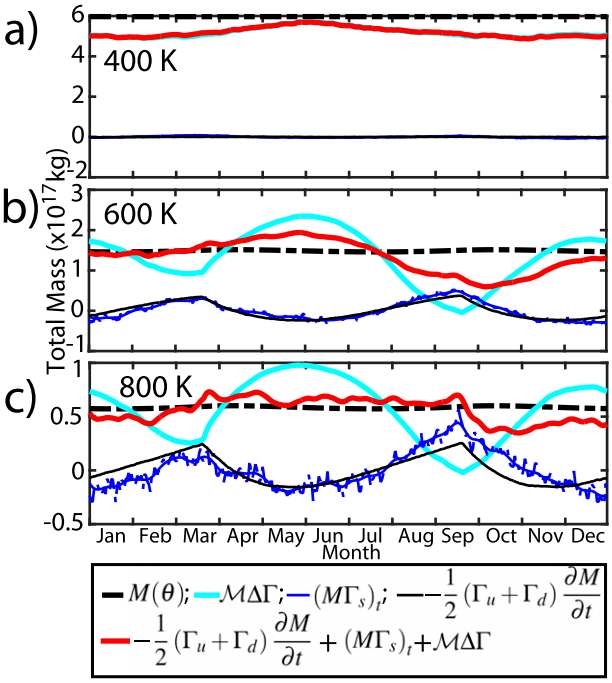

FIG. 5. Twenty years of model output have been averaged at each day of the year to produce a climatological seasonal cycle for the different terms in the age budget: $M(\theta) = \mathcal{M}\Delta\Gamma + (M\Gamma_s)_t + [-(\Gamma_u + \Gamma_d)M_t/2]$. Each panel shows the individual terms and the right-hand side at a different level: (a) 400, (b) 600, and (c) 800 K.

different levels in Fig. 5. At 400 K, shown in Fig. 5a, in the very low stratosphere, there is very little effect of the seasonal cycle. The product of the overturning strength and the age difference $\mathcal{M}\Delta\Gamma$ is at all times less than the total mass M. This discrepancy will be addressed in section 3f. The time-derivative terms are small. At 600 K, shown in Fig. 5b, the seasonal cycle is much more pronounced, and here the difference between $\mathcal{M}\Delta\Gamma$ and the total mass above the isentrope has a stronger variation in time. The time-derivative terms are approximately the same magnitude, but the variability in $(M\Gamma_s)_t$ is much greater: it has been smoothed with a binomial filter before contributing to the sum. The sum of $\mathcal{M}\Delta\Gamma + (M\Gamma_s)_t + -(\Gamma_u + \Gamma_d)M_t/2$ is closer to the total mass above the isentrope $M(\theta)$, and by including the time-dependent terms, the seasonal variation is decreased. Significant discrepancies remain, however. At 800 K, shown in Fig. 5c, the balance holds even more closely, as the sum is quite close to the total mass for most of the year.

Because of the strong temporal variability, it is clear that the steady-state theory cannot be applied instantaneously. The contributions of the time-derivative terms are smaller upon long-term averaging, however. The magnitude of the annual average of these terms is shown as a percentage of the total mass above each isentrope in

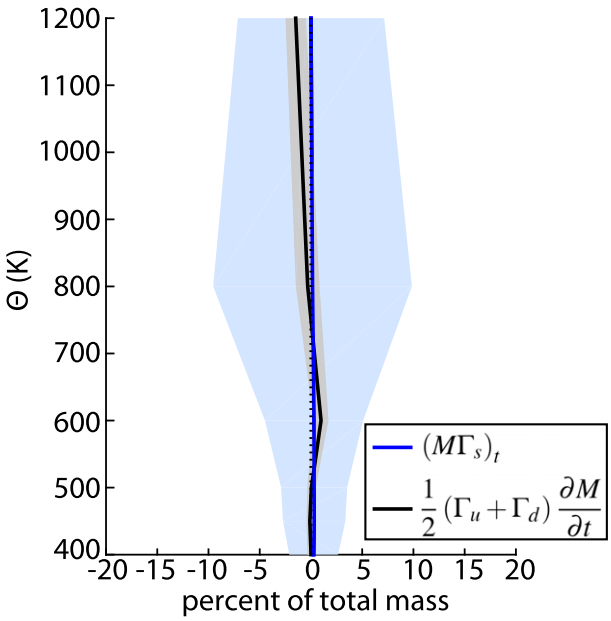

FIG. 6. The fractional contribution of the annually averaged time-dependent terms in (26) as a percentage of the total mass above the isentrope (solid lines) with the standard deviation of the annual averages (shading). The blue is $(M\Gamma_s)_t/M \times 100\%$, and the black/gray is $(\Gamma_u + \Gamma_d)M_t/2/M \times 100\%$.

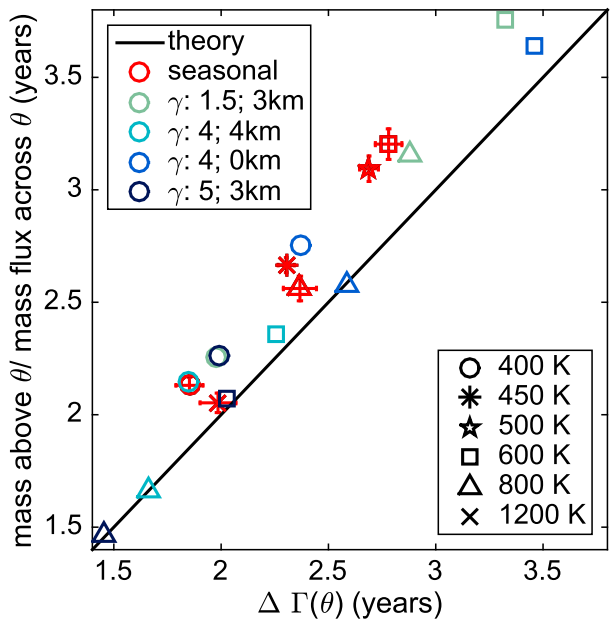

FIG. 7. The ratio of mass above an isentrope to mass flux through an isentrope vs the difference between downwelling and upwelling age of air on the isentrope. The green and blue points are averages from the last 2000 days of perpetual-solstice runs, as described in Table 1. The red points are the average of 50 annual averages from the seasonally varying run with 4000-m topography and lapse rate of 4 K km^{-1}. The error bars are one standard deviation of the annual averages. The black line shows the one-to-one relationship predicted by the theory, and the different symbols are different isentropic levels.

the solid lines in Fig. 6, and the standard deviation is shown in the shading. As we already observed from Fig. 5, the variability of $(M\Gamma_s)_t$ is much greater than that of $(\Gamma_u + \Gamma_d)M_t/2$, up to 10% of $M(\theta)$. The long-term averages of both terms are small. In Fig. 7, we compare the annual averages of $M/\mathcal{M}$ and $\Delta\Gamma$. The mean of 50 yr from the seasonally varying model run is in the red points, with the error bars showing the standard deviation of the annual means. The blue and green points are from the variety of model runs in perpetual-solstice scenarios, as enumerated in Table 1. These steady-state runs represent a wide range of climates, with the mass flux across the 600-K surface varying by a factor of about 2. As the total mass above each surface does not change much between the simulations, this results in a factor of 2 in the age difference as well. Examining the blue and green points shows that the theory holds across the whole range of climates simulated here. The annual averages from the seasonally varying model run result in as good agreement with the steady-state theory as the perpetual-solstice model runs, so we conclude that the annual-average overturning strength can be determined by the annual average of the age difference and of the mass above the isentrope.

e. *Area-weighted averaging*

This theory has been developed, by necessity, using mass-flux-weighted age of air. This precludes applying the theory directly to age data, because the circulation is unknown. We therefore try here to determine the bias introduced by using area-weighted age of air rather than mass-flux-weighted age of air. To do this, we define regions of upwelling and downwelling and take the area-weighted average of age in those regions. Because age of air data alone will not inform us as to the upwelling and downwelling regions, we also perform the averaging for the same "upwelling" and "downwelling" regions as for the time-average results (constant latitude bands). The bias introduced by this averaging in the seasonally varying model is shown at different levels in Fig. 8, where we show this bias as a fraction of the mass-flux-weighted age difference. The area-weighted age difference is smaller than the mass-flux-weighted age difference in all cases. Using the "true" upwelling and downwelling regions gives a bias of about 10%–15%, and the 40° band is similar. When the regions get farther from the "true" upwelling and downwelling, the bias becomes greater. In this model, the bias is quite consistent from year to year, as can be seen by the narrow range spanned by one standard deviation from the mean. This investigation demonstrates that we can qualitatively think about the

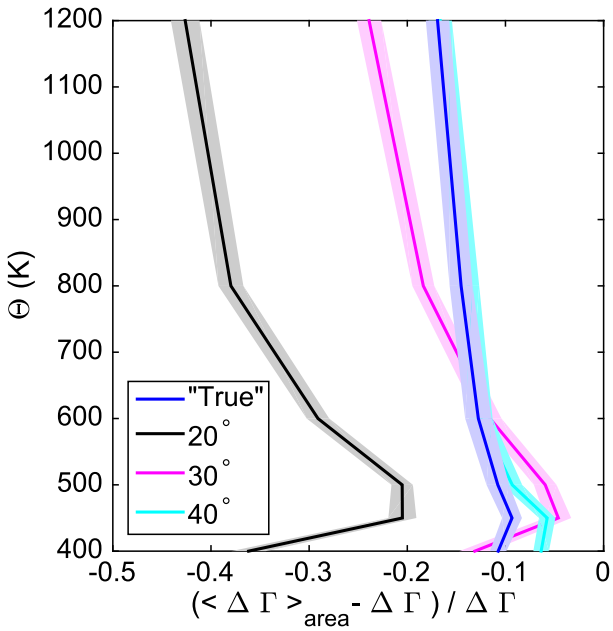

FIG. 8. The bias introduced by using area-weighted age difference rather than mass-flux-weighted age difference for different regions. The shading shows one standard deviation of the annual average for 50 yr of the seasonally varying model run. The overturning regions are defined as in Fig. 3. The blue shows the "true" region, the black shows the 20°S–20°N upwelling region, the magenta shows the 30°S–30°N upwelling region, and cyan 40°S–40°N upwelling region.

age difference on an isentrope as a proxy for the diabatic circulation through that isentrope.

f. The role of diabatic diffusion

As in Fig. 3, the points in Fig. 7 all fall above the one-to-one line, implying that the actual age difference is less than that predicted by the theory by up to about 15%. In the time-average case there is nothing to account for this discrepancy, and in Fig. 7 the discrepancy is too great to be explained by the time average of the transient terms. Therefore, the discrepancy must arise from terms missing from the theory. Diabatic mixing was neglected at the outset. If we revisit that assumption and include a diffusion of age in (4), we obtain

$$\int_\theta \sigma\dot{\theta}\Gamma\, dA - \int_\theta \sigma K_{\theta\theta}\frac{\partial\Gamma}{\partial\theta}\, dA = -M \tag{31}$$

or

$$\mathcal{M}\Delta\Gamma + \int_\theta \sigma K_{\theta\theta}\frac{\partial\Gamma}{\partial\theta}\, dA = M, \tag{32}$$

where $K_{\theta\theta}$ is the diffusivity. Because of adiabatic mixing in this model, age increases with increasing θ in all latitudes and altitudes considered here. Since $K_{\theta\theta}$ is positive, the diffusion is a positive term on the left side. In panel Figure 5a we noted that the product of the overturning mass flux and the age difference was always less than the total mass above 400 K. Now we see that this difference is consistent with the neglect of diffusion. Similarly, the contribution from the diffusive term would account for age differences lower than the theory predicts in both Figs. 3 and 7. To determine whether the diffusivity $K_{\theta\theta}$ necessary to close the age budget is reasonable, we assume constant diffusivity and find that, at 450 K, $K_{\theta\theta} \approx 1.7 \times 10^{-5}\,\mathrm{K^2\,s^{-1}}$. Given the background stratification in the model, this corresponds to about $K_{zz} \simeq 0.1\,\mathrm{m^2\,s^{-1}}$, a value that is consistent with observational studies (Sparling et al. 1997; Legras et al. 2003).

In the real world, small-scale diffusion will provide a diabatic component of the age flux, but the model has no representation of such processes, so they cannot be a factor here. However, the large-scale motions are not, as was assumed in the derivation, strictly adiabatic but will exhibit "diabatic dispersion" (Sparling et al. 1997; Plumb 2007). We can estimate the diffusivity based on Plumb (2007):

$$K_{\theta\theta} \sim |\dot{\theta}'|^2 \tau_{\mathrm{mixing}}, \tag{33}$$

where τ_{mixing} is the time scale for isentropic mixing across the surf zone. For the purposes of this estimate, we use the deviation of $\dot{\theta}$ from the zonal mean as an approximation for $\dot{\theta}'$ and use $\tau_{\mathrm{mixing}} \approx 30$ days. Using an average value for $|\dot{\theta}'|^2$ in Northern Hemisphere midlatitudes at 450 K from the seasonally varying model run gives $K_{\theta\theta} \approx 1 \times 10^{-5}\,\mathrm{K^2\,s^{-1}}$. The diabatic dispersion is thus close to the diffusivity necessary to close the age budget in this simple model. Now, revisiting the observation that the points on the 800-K isentrope seem to have better agreement with the theory line in Fig. 3, we can understand this as the effect of the reduced cross-isentropic gradient of age higher up in the stratosphere. The same diabatic diffusivity will therefore result in less diffusion of age because of the smaller gradient, and the calculated age difference will better match the theory.

4. Summary and conclusions

The theoretical developments in this paper have focused on extension of the simple relationship between the gross latitudinal age gradient on isentropes and the diabatic circulation, obtained by Neu and Plumb (1999) for the "leaky tropical pipe" model. Under their assumptions of steady state and no diabatic mixing, but without any "tropical pipe" construct, an essentially identical result follows. We then show that the result

survives intact when applied to time averages of an unsteady situation but does not apply locally in time. The predicted age gradient is independent of isentropic mixing and of the structure of the circulation above the level in question.

Analysis of results from a simplified global model, in both perpetual solstice and fully seasonal configurations, shows that the time-averaged result holds quite well, although the predicted age difference overestimates the actual value by up to 15%, a fact that we ascribe to the neglect of large-scale diabatic mixing in the theory. Indeed, estimates of diabatic dispersion in the model are sufficient to account for the discrepancy.

The theory is, of necessity, formulated in entropy (potential temperature) coordinates, and consequently it is the diabatic circulation (rather than, say, the residual circulation) that is related to the latitudinal structure of age. While these two measures of the circulation can, at times (especially around the equinoxes), be very different, in the long-term average to which this theory applies they are essentially identical.

The relationship between age gradient and the circulation is straightforward, but in order to use age data to deduce the circulation there are some subtleties: in order to quantify the mean age difference, in principle one needs to know the geometry of the mean upwelling and downwelling regions and the spatial structure of the circulation (since, strictly, it is the mass-flux-weighted mean that is required). The theoretical result is unchanged if simpler regions (such as equatorward and poleward of, say, 30°) are used instead of those of upwelling/downwelling, but of course the mass flux involved is that within each chosen region, rather than the total overturning mass flux. When we test the agreement of the theory using an area-weighted age difference using the "true" upwelling and downwelling regions, this introduces a bias of 10%–15% underestimation of the magnitude of the age difference, with a smaller bias lower in the stratosphere. Using 40°S–40°N as the upwelling region and the rest of the globe as the downwelling region, which is a calculation that is possible entirely from data, we find that the area-weighted age difference has a similar underestimation of the mass-flux-weighted age difference as using the "true" regions. The area-weighted age difference can therefore be used to infer the circulation qualitatively, since the difference is only up to 15%. We caution that this bias estimate was performed with the simple idealized model, and, to get a quantitative estimate of the overturning circulation strength from data, a more realistic model is necessary and other factors must be considered.

Despite these caveats, these results offer an avenue for identifying trends in the circulation by seeking trends in age data, as done by Haenel et al. (2015) and Ploeger et al. (2015b). For one thing, the theory shows that it is the gross isentropic age difference, and not the age itself, that is related to the strength of the circulation. For another, these results show that annual averages (at least) are necessary to relate the strength of the circulation to the age, so good data coverage in space and time is necessary to eliminate the seasonal variability for which the theory is not applicable. It will require an accumulation of a long time series of global measurements to separate the long-term trends in the circulation from the short-term variability.

Acknowledgments. We thank S.-J. Lin and Isaac Held for providing the GFDL AM3 core. This research was conducted with government support for ML under and awarded by the DoD, Air Force Office of Scientific Research, National Defense Science and Engineering Graduate (NDSEG) Fellowship, 32 CFR 168a. Funding for AS was provided by a Junior Fellow award from the Simons Foundation. This work was also supported in part by the National Science Foundation Grants AGS-1547733 to MIT and AGS-1546585 to NYU.

REFERENCES

Abalos, M., B. Legras, F. Ploeger, and W. J. Randel, 2015: Evaluating the advective Brewer–Dobson circulation in three reanalyses for the period 1979–2012. *J. Geophys. Res. Atmos.*, **120**, 7534–7554, doi:10.1002/2015JD023182.

Butchart, N., 2014: The Brewer–Dobson circulation. *Rev. Geophys.*, **52**, 157–184, doi:10.1002/2013RG000448.

——, and Coauthors, 2006: Simulations of anthropogenic change in the strength of the Brewer–Dobson circulation. *Climate Dyn.*, **27**, 727–741, doi:10.1007/s00382-006-0162-4.

——, and Coauthors, 2011: Multimodel climate and variability of the stratosphere. *J. Geophys. Res.*, **116**, D05102, doi:10.1029/2010JD014995.

Donner, L. J., and Coauthors, 2011: The dynamical core, physical parameterizations, and basic simulation characteristics of the atmospheric component AM3 of the GFDL global coupled model CM3. *J. Climate*, **24**, 3484–3519, doi:10.1175/2011JCLI3955.1.

Engel, A., and Coauthors, 2009: Age of stratospheric air unchanged within uncertainties over the past 30 years. *Nat. Geosci.*, **2**, 28–31, doi:10.1038/ngeo388.

Fu, Q., P. Lin, S. Solomon, and D. L. Hartmann, 2015: Observational evidence of strengthening of the Brewer–Dobson circulation since 1980. *J. Geophys. Res. Atmos.*, **120**, 10 214–10 228, doi:10.1002/2015JD023657.

Garcia, R. R., W. J. Randel, and D. E. Kinnison, 2011: On the determination of age of air trends from atmospheric trace species. *J. Atmos. Sci.*, **68**, 139–154, doi:10.1175/2010JAS3527.1.

Garny, H., T. Birner, H. Boenisch, and F. Bunzel, 2014: The effects of mixing on age of air. *J. Geophys. Res. Atmos.*, **119**, 7015–7034, doi:10.1002/2013JD021417.

Gerber, E. P., 2012: Stratospheric versus tropospheric control of the strength and structure of the Brewer–Dobson circulation. *J. Atmos. Sci.*, **69**, 2857–2877, doi:10.1175/JAS-D-11-0341.1.

——, and L. M. Polvani, 2009: Stratosphere–troposphere coupling in a relatively simple AGCM: The importance of stratospheric variability. *J. Climate*, **22**, 1920–1933, doi:10.1175/2008JCLI2548.1.

Haenel, F. J., and Coauthors, 2015: Reassessment of MIPAS age of air trends and variability. *Atmos. Chem. Phys.*, **15**, 13 161–13 176, doi:10.5194/acp-15-13161-2015.

Hall, T. M., and R. A. Plumb, 1994: Age as a diagnostic of stratospheric transport. *J. Geophys. Res.*, **99**, 1059–1070, doi:10.1029/93JD03192.

——, D. W. Waugh, K. A. Boering, and R. A. Plumb, 1999: Evaluation of transport in stratospheric models. *J. Geophys. Res.*, **104**, 18 815–18 839, doi:10.1029/1999JD900226.

Hardiman, S. C., N. Butchart, and N. Calvo, 2014: The morphology of the Brewer–Dobson circulation and its response to climate change in CMIP5 simulations. *Quart. J. Roy. Meteor. Soc.*, **140**, 1958–1965, doi:10.1002/qj.2258.

Held, I. M., and M. J. Suarez, 1994: A proposal for the intercomparison of the dynamical cores of atmospheric general circulation models. *Bull. Amer. Meteor. Soc.*, **75**, 1825–1830, doi:10.1175/1520-0477(1994)075<1825:APFTIO>2.0.CO;2.

Kushner, P. J., and L. M. Polvani, 2006: Stratosphere–troposphere coupling in a relatively simple AGCM: Impact of the seasonal cycle. *J. Climate*, **19**, 5721–5727, doi:10.1175/JCLI4007.1.

Legras, B., B. Joseph, and F. Lefèvre, 2003: Vertical diffusivity in the lower stratosphere from Lagrangian back-trajectory reconstructions of ozone profiles. *J. Geophys. Res.*, **108**, 4562, doi:10.1029/2002JD003045.

Neu, J. L., and R. A. Plumb, 1999: Age of air in a "leaky pipe" model of stratospheric transport. *J. Geophys. Res.*, **104**, 19 243–19 255, doi:10.1029/1999JD900251.

Oberländer-Hayn, S., and Coauthors, 2016: Is the Brewer–Dobson circulation increasing or moving upward? *Geophys. Res. Lett.*, **43**, 1772–1779, doi:10.1002/2015GL067545.

Ploeger, F., M. Abalos, T. Birner, P. Konopka, B. Legras, R. Müller, and M. Riese, 2015a: Quantifying the effects of mixing and residual circulation on trends of stratospheric mean age of air. *Geophys. Res. Lett.*, **42**, 2047–2054, doi:10.1002/2014GL062927.

——, M. Riese, F. Haenel, P. Konopka, R. Müller, and G. Stiller, 2015b: Variability of stratospheric mean age of air and of the local effects of residual circulation and eddy mixing. *J. Geophys. Res. Atmos.*, **120**, 716–733, doi:10.1002/2014JD022468.

Plumb, R. A., 2002: Stratospheric transport. *J. Meteor. Soc. Japan*, **80**, 793–809, doi:10.2151/jmsj.80.793.

——, 2007: Tracer interrelationships in the stratosphere. *Rev. Geophys.*, **45**, RG4005, doi:10.1029/2005RG000179.

Polvani, L. M., and P. J. Kushner, 2002: Tropospheric response to stratospheric perturbations in a relatively simple general circulation model. *Geophys. Res. Lett.*, **29**, 40–43, doi:10.1029/2001GL014284.

Putman, W. M., and S.-J. Lin, 2007: Finite-volume transport on various cubed-sphere grids. *J. Comput. Phys.*, **227**, 55–78, doi:10.1016/j.jcp.2007.07.022.

Ray, E. A., and Coauthors, 2010: Evidence for changes in stratospheric transport and mixing over the past three decades based on multiple data sets and tropical leaky pipe analysis. *J. Geophys. Res.*, **115**, D21304, doi:10.1029/2010JD014206.

Sheshadri, A., R. A. Plumb, and E. P. Gerber, 2015: Seasonal variability of the polar stratospheric vortex in an idealized AGCM with varying tropospheric wave forcing. *J. Atmos. Sci.*, **72**, 2248–2266, doi:10.1175/JAS-D-14-0191.1.

Singh, M. S., and P. A. O'Gorman, 2012: Upward shift of the atmospheric general circulation under global warming: Theory and simulations. *J. Climate*, **25**, 8259–8276, doi:10.1175/JCLI-D-11-00699.1.

Sparling, L. C., J. A. Kettleborough, P. H. Haynes, M. E. McIntyre, J. E. Rosenfield, M. R. Schoeberl, and P. A. Newman, 1997: Diabatic cross-isentropic dispersion in the lower stratosphere. *J. Geophys. Res.*, **102**, 25 817–25 829, doi:10.1029/97JD01968.

Stiller, G. P., and Coauthors, 2012: Observed temporal evolution of global mean age of stratospheric air for the 2002 to 2010 period. *Atmos. Chem. Phys.*, **12**, 3311–3331, doi:10.5194/acp-12-3311-2012.

Strahan, S. E., and Coauthors, 2011: Using transport diagnostics to understand chemistry climate model ozone simulations. *J. Geophys. Res.*, **116**, D17302, doi:10.1029/2010JD015360.

Volk, C. M., and Coauthors, 1997: Evaluation of source gas lifetimes from stratospheric observations. *J. Geophys. Res.*, **102**, 25 543–25 564, doi:10.1029/97JD02215.

Waugh, D., and T. M. Hall, 2002: Age of stratospheric air: Theory, observations, and models. *Rev. Geophys.*, **40**, 1010, doi:10.1029/2000RG000101.